Experimental and computational study on heat transfer of a 150 kW aircooled eddy current dynamometer

by Nazaruddin Sinaga

Submission date: 10-Jan-2020 10:15AM (UTC+0700)
Submission ID: 1240522140
File name: 3.pdf (8.37M)
Word count: 3259
Character count: 17433

Experimental and computational study on heat transfer of a 150 kW air-cooled eddy current dynamometer

Experimental and computational study on heat transfer of a 150 kW air-cooled eddy current dynamometer

Nazaruddin Sinaga[1,*] Syaiful[1], B Yunianto[1] and M Rifal[2]

1. Introduction

To run an energy efficiency program and an environmentally friendly transportation system, a dynamometer is needed to determine the fuel economy, in units of km/liter, and the emissions of a vehicle, in units of gr/km. When measuring these two quantities, the vehicle is running on a chassis dynamometer by following a driving scenario called the driving cycle. To be able to run this driving cycle, the vehicle must be loaded by a dynamometer. Recently, there are almost no workshops or vehicle dealers in Indonesia that use dynamometer for the purposes mentioned above. This is because the price of a dynamometer is relatively expensive, particularly for small-scale workshops, because there has been no dynamometer manufacturer in the country.

The Eddy current dynamometer works according to Faraday's law of electromagnetic induction [1]. According to this law, whenever a conductor cuts magnetic lines of forces, an emf is induced in the conductor, the magnitude of which is proportional to the strength of the magnetic field and the speed of the conductor. If the conductor is a disc, there will be circulated eddy currents in the disc. According to Lenz's law, the direction of the current is in such a way as to oppose the movement of the disc [2].

Essentially the eddy current brake consists of two components, a stationary magnetic field system, and a solid rotating part, which include a metal disc [3, 4] as shown in image 1 and 2. The rotor, generally

of mild steel, sometimes referred to as the secondary because the eddy currents are induced. The stator consists of pole core, pole shoe, and winding coil. The coil is wounded at the pole core, where copper or aluminum is used for winding material. The pole core and shoe are made of mild steel and fixed with a bolt and screw. The stator and rotor are separated by a close air gap for torque transmission. During braking, the metal disc is exposed to a magnetic field by the coils and generates eddy currents in the disc. The interaction between the magnetic field and the eddy currents slow down the rotating disc [5]. Consequently, there is no wear as in the friction brake.

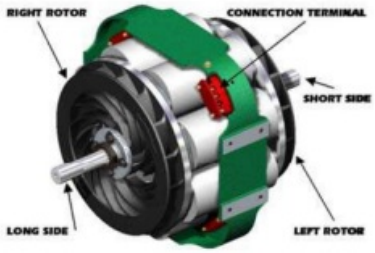

Figure 1. The KLAM CFK-140 Power Absorber Unit produced by Industrial Zelu [3]

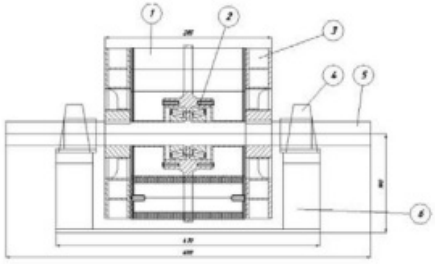

Figure 2. The main parts of dynamometer: (1) solenoid; (2) stator; (3) rotor; (4) pillow block bearing; (5) shaft; (6) frame [4]

Air-cooled eddy current dynamometer is one of the instruments employed to evaluate the power and torque of a rotating engine. Even though there is no surface wear, all of these parts will receive a high amount of heat due to braking. If the cooling system is inadequate, then the stator and rotor surface will experience a high increase in temperature. The temperature rise on both stator and rotor surfaces of the air-cooled dynamometer will drop the dynamometer capacity as low as 70% [6]. To resolve this issue, it needs a system that has a high cooling rate. Therefore, efforts need to be made to increase the cooling rate of the air-cooled eddy current dynamometers. It could be realized by optimizing the dynamometer design using artificial neural networks [7, 8] or other methods. However, the optimization is complicated because it involves many parameters [9, 10, 11].

Since the heat transfer mechanism is very complicated and has several parameters affecting the cooling rate, it is advantageous to study the phenomena theoretically, by using the computational method. With the help of this computational software, calculations can be done quickly. However, the

accuracy of the results of these theoretical calculations must first be justified so that the results have low uncertainty. When a precise calculation model has been obtained, the effect of various design parameters from the dynamometer can be searched quickly. This research was conducted in order to obtain a calculation model that can be used to perform optimal design of the air-cooled eddy current dynamometer. The primary objective of this study is to validate the numerical simulation modeling by experimental results. The finite volume method, facilitated by ANSYS FLUENT® software, is used to solve the problem.

2. Methodology

Measurements in the laboratory were carried out by running a dynamometer on a chassis dynamometer at several load values and dynamometer rotational speed. Table 1 shows the main dimensions of the dynamometer being tested, while figure 3 shows the measurement system. Measurements is begun after the dynamometer reached a steady state. At each loading, a rotor surface temperature measurement and flow discharge through the outlet side of the rotor are measured. The next measurement results are compared with the results of numerical calculations. To be able to produce a large enough load, the Toyota Fortuner car has a maximum torque of 400 Nm at 5000 rpm and a maximum power of 125 kW at a speed of 4500 rpm. In figure 2 above shows the construction of a dynamometer in the Efficiency and Energy Conservation Laboratory of Mechanical Engineering Department, Diponegoro University. In this study, eighteen simulations were carried out by varying four types of turbulence models, discretization of first and second order momentum, and three types of discretization of Pressure Velocity Coupling. The turbulence model used is the turbulence model k-ε standard, k-ε RNG, k-ε realizable, and Spalart-Allmaras.

Table 1. Specification of eddy current dynamometer [12]

Parameter	Value
Outer diameter (D_1)	290 mm
Inner diameter (D_2)	140 mm
Inlet blade angle (β_1)	64°
Outlet blade angle (β_2)	26°
Blade number	16
Blade width (b)	50 mm

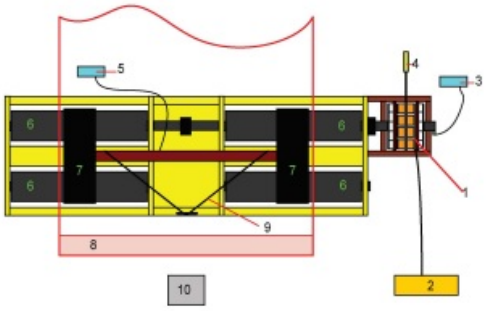

Figure 3. Measurement system: (1) dynamometer; (2) power supply; (3) dyno tachometer; (4) load cell; (5) wheel tachometer; (6) chassis roller; (7) car wheels; (8) car; (9) straps; (10) cooling fan

In this study, the method used is a computational approach, namely the finite volume method. This is a method that is widely used in solving fluid flow and heat transfer problems numerically. In the finite volume method, unknown variables are explained using a specific point on the nodal points. Generally,

the basic procedures for solving problems using the finite volume method are as follows: estimating the value of unknown flow variables using a simple function; make a discretization equation by entering the estimation into the general equation of flow, and then doing mathematical manipulation; and finally solve the algebraic equation of the problem at hand [13]. Currently, there is quite several computational fluid dynamic software that can be used to solve flow problems and heat transfer. In this study, ANSYS FLUENT® software is used. One of the advantages of the software is its complete literature and is very widely used in scientific. Besides, this software also has complete features.

3. Turbulence Models

In FLUENT, several turbulence models can be simulated, including the k-ε standard model, k-ε RNG, and k-ε realizable and Spalart-Allmaras. All of these models have a similar shape because they contain transport equations for k (turbulent kinetic energy) and ε (turbulent energy dissipation).

3.1. k-ε Standard

The k-ε standard model is a semi-empirical model compiled based on the transport equation for turbulent kinetic energy and turbulent dissipation energy. In the model k-ε it is assumed that the flow is fully turbulent, and the effect of molecular viscosity is negligible. Therefore this model is only suitable for fully turbulent flow. The turbulent kinetic energy, k and the rate of dissipation ε are obtained from the following equation:

$$\rho\frac{Dk}{Dt} = \frac{\partial}{\partial x_i}\left[\left(\mu + \frac{\mu_t}{\sigma_k}\right)\frac{\partial k}{\partial x_i}\right] + G_k + G_b - \rho\epsilon - Y_M \quad (1)$$

$$\rho\frac{D\epsilon}{Dt} = \frac{\partial}{\partial x_i}\left[\left(\mu + \frac{\mu_t}{\sigma_\epsilon}\right)\frac{\partial \epsilon}{\partial x_i}\right] + C_{1\epsilon}\frac{\epsilon}{k}(G_k + C_{3\epsilon}G_b) - C_{2\epsilon}\rho\frac{\epsilon^2}{k} \quad (2)$$

3.2. k-ε RNG

This turbulence model is derived from the Navier-Stokes equation using a mathematical technique called the renormalization group method. Model k-ε RNG has a shape similar to the k-ε standard model as follows.

$$\rho\frac{Dk}{Dt} = \frac{\partial}{\partial x_i}\left(\alpha_k\mu_{eff}\frac{\partial k}{\partial x_i}\right) + G_k + G_b - \rho\epsilon - Y_M \quad (3)$$

$$\rho\frac{D\epsilon}{Dt} = \frac{\partial}{\partial x_i}\left(\alpha_\epsilon\mu_{eff}\frac{\partial \epsilon}{\partial x_i}\right) + C_{1\epsilon}\frac{\epsilon}{k}(G_k + C_{3\epsilon}G_b) - C_{2\epsilon}\rho\frac{\epsilon^2}{k} - R \quad (4)$$

3.3. k-ε Realizable

The term realizable means that this model meets certain limitations of normal stress, which is consistent with the physical properties of turbulent flow. By combining the Boussinesq relationship and the definition of turbulent viscosity, a normal Reynolds stress can be obtained in an incompressible flow. The transport equation for the k-ε realizable is as follows.

$$\rho\frac{Dk}{Dt}=\frac{\partial}{\partial x_j}\left[\left(\mu+\frac{\mu_t}{\sigma_k}\right)\frac{\partial k}{\partial x_j}\right]+G_k+G_b-\rho\epsilon-Y_M \quad (5)$$

$$\rho\frac{D\epsilon}{Dt}=\frac{\partial}{\partial x_j}\left[\left(\mu+\frac{\mu_t}{\sigma_\epsilon}\right)\frac{\partial \epsilon}{\partial x_j}\right]+\rho C_1 S\epsilon-\rho C_2\frac{\epsilon^2}{k+\sqrt{\nu\epsilon}}+C_{1\epsilon}\frac{\epsilon}{k}C_{3\epsilon}G_b \quad (6)$$

3.4. *Spalart-Allmaras*

The transported variable in the Spalart-Allmaras model, ν, is identical to the turbulent kinematic viscosity except in the near-wall (viscosity-affected) region. The transport equation for the modified turbulent viscosity ν is

$$\frac{\partial}{\partial t}(\rho\tilde{\nu})+\frac{\partial}{\partial x_i}(\rho\tilde{\nu}u_i)=G_\nu+\frac{1}{\sigma_{\tilde{\nu}}}\left[\frac{\partial}{\partial x_j}\left\{(\mu+\rho\tilde{\nu})\frac{\partial\tilde{\nu}}{\partial x_j}\right\}+C_{b2}\rho\left(\frac{\partial\tilde{\nu}}{\partial x_j}\right)^2\right]-Y_\nu+S_{\tilde{\nu}} \quad (7)$$

where G_ν is the production of turbulent viscosity, and Y_ν is the destruction of turbulent viscosity that occurs in the near-wall region due to the wall blocking and viscous damping. σ_ν and C_{b2} are the constants and ν is the molecular kinematic viscosity. S_ν is a user-defined source term. Note that since the turbulence kinetic energy, k, is not calculated in the Spalart-Allmaras model, the last term in the equation is ignored when estimating the Reynolds stresses.

4. Simulation Process

4.1. *Problem Description*

The problem involves modeling the steady-state flow of air through a centrifugal blower running at 1500 rpm. There are 16 blade rows in this blower. To simplify the CFD calculation, the flow is modeled only through double blade rows and uses rotationally periodic boundary conditions on the boundaries between the blade rows. The governing equations are cast in a Single Reference Frame moving at the speed of the rotor. Air is treated as an ideal gas with constant values of specific heat, thermal conductivity, and dynamic viscosity. The schematic of double blade rows and the complete rotor, repeating a single blade row 16 times, are shown in figure 4.

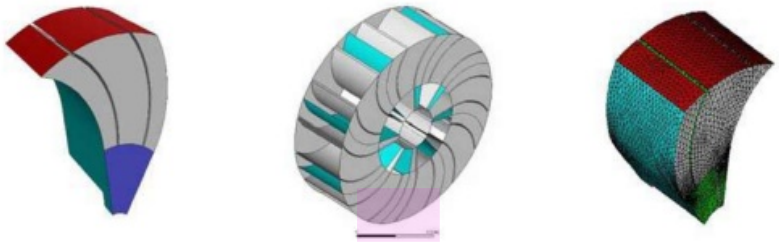

(a) (b) (c)

Figure 4. (a) calculated geometry; (b) full rotor geometry; (c) meshing on the domain geometry

4.2. Domain Geometry

In the present calculation, the rotor plate outer diameter is 290 mm, the inner diameter of the front rotor plate is 140 mm, the number of blades is 16 pieces, and the rotor material is made of St 60 steel. The blade width is 50mm, with the rotor blade entry angle are 64°, while the blade exit angle is 26°.

4.3. Numerical Scheme

There are two numerical schemes provided by FLUENT, namely segregated and coupled solvers. FLUENT solves general integral equations for mass, momentum, energy and other scalar quantities such as turbulence. Both of these numerical schemes use the same discretization process, namely finite volume methods. The only difference lies in the approach used in linearizing and solving discrete equations. The approach taken by coupled methods is to solve continuity, momentum, and energy equations simultaneously.

4.4. Model and Materials

As a first step in the modeling in ANSYS FLUENT, we have to set up the general model as follows: enable the density-based, steady-state solver and retain the default values for the other parameters. The second step is to enable the Spalart-Allmaras turbulence model, and retain the default values for the other parameters. The Spalart-Allmaras turbulence model is an excellent and economical choice for mildly complex boundary-layer flows in turbomachinery. The next step is to set the density of air to ideal-gas. The ideal gas model will automatically enable the solution of the energy equation. For simplicity, we will keep the other fluid properties at their default constant values, though they could be made the function of temperature if desired.

4.5. Boundary Conditions

In figure 5, a cell zone conditions setting is shown in the blade area, which is then given a rotational speed with a specific value in the rotational velocity, for example, 1500 rpm. In this inlet area, the pressure is 1000 Pa gauge, and the initial gauge pressure is 1000 Pa, while the turbulent viscosity ratio is 10. The outlet condition is a pressure outlet of 1000 Pa, and the turbulent viscosity ratio backflow is 10. Figure 5 also shown the boundary conditions at the hub, shaft, shroud-b, and shroud-d areas, where the wall is a moving wall, relative to adjacent cell zone with the rotational axis is X = 1, and rotational speed is zero. For wall boundary conditions of blade1-p, blade1-s, blade2-p, and blade2-s, the settings are the same as before.

4.6. Solver Discretization, Controls, and Monitors

Retain the default solution methods for flow under solve methods, and set the turbulence equation to second order upwind. Activate the pseudo transient method then retain the default solution controls under solving controls. For the residual convergence, set the convergence criterion for continuity to 1e-5. Create three surface monitors as follows: mass flow rate at the inlet, the mass flow rate at the outlet, and mass-averaged total pressure at the outlet.

Table 1. Boundary conditions in inlet and outlet

Name	Boundary Conditions	Label
Inlet-D	Intake Fan	A
Inlet-B	Intake Fan	B
Outlet	Exhaust Fan	C
Hub	wall	D
Shroud-D	wall	E
Shroud-B	wall	F
Blade1-P	wall	H
Blade1-S	wall	I
Blade2-P	wall	J

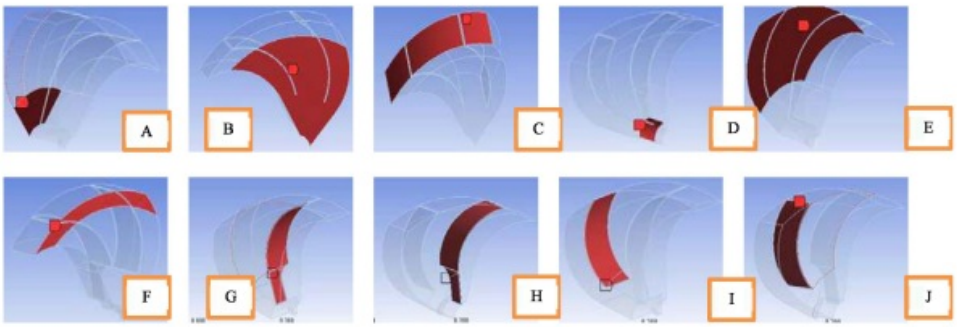

Figure 5. Boundary conditions on inlet-B, D, outlet, and wall

5. Analysis and Discussion

Four turbulence models with standard wall models have been tried in this simulation, using fixed material properties. Initial price initialization is given at the cylinder flow rate. The gathering process is carried out in the following order:

a) The initial grid is simulated until it converges using first-order discretization momentum
b) The results above are refined by using a second-order momentum schematization
c) Smoothing the grid is carried out with adaptive facilities for areas that have a high gradient of velocity, pressure, and kinetic energy. Cells that have Y^+ values smaller than ten are not adapted so that the first cell is not too close to the wall in a standard wall function model.

In this study, 18 simulations were carried out by varying three types of turbulence models, discretization of first and second order momentum, and three types of discretization of PVC (Pressure Velocity Coupling). The purpose of the simulation by varying the three options above is intended to determine the level of convergence of the iteration process and the time required in the calculation. The results of the next calculation are compared with the experimental results. From the comparison of all simulations carried out the results show that the calculation with the Realizable k-ε turbulence model cannot be converged if it uses the second discretization momentum and the PISO. This model can converge with the second order if the SIMPLE method is used. Although the amount and time of the iteration required vary, it turns out that the calculations produced by each simulation process are not much different. The accuracy of the calculation results, according to the properties of this numeric method, will be higher using the second order discretion. When viewed from the number of iterations and the time required, it can be concluded that the use of the PISO method can provide faster calculation results with a smaller number of iterations.

From the comparison of the turbulence model, discretization of momentum, and discretization of PVC that has been done and the description above, in general, it can be said that the three parameters can provide the results of convergent calculations. The effect of discretization of momentum seems not too large, only adds accuracy to the calculation. The influence of turbulence and discretization models of PVC plays a significant role in the correctness of the calculation results. Although not explicitly discussed here, it can be said that the use of the turbulence model that gives the best results is the Spalart-Allmaras model, as seen in figure 6. Discretization of SIMPLE and PISO generally produces almost the same effect even though the number and duration of the iteration process will be affected. Therefore from the results of this study, it is recommended to use the Splart-Allmaras model, which is combined with the PISO discretization and 2nd-order momentum, as a model to study the flow phenomenon in air-cooled dynamometer rotors.

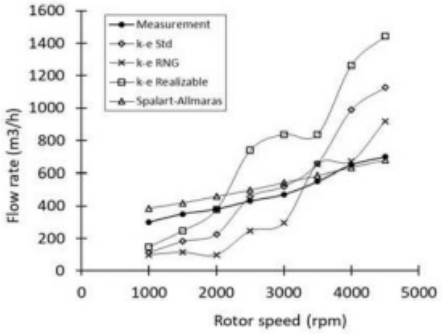

Figure 6. Comparison of experimental and computational results

Figure 7 shows the effect of rotor speed on flow discharge at the front and rear inlet and outlet for optimal blade geometry using the Spalart-Allmaras model. In this case, the blade width is 90 mm, blade inlet angle 73 degrees and the blade outlet angle is 26 degrees. It can be seen that the effect of the rotor speed on the flow rate is linear; that is, the faster the rotor speed, the higher the flow rate. It can be seen that the lowest line gradient is at the flow discharge that enters the rear inlet side. Therefore, it can be concluded that the effect of rotor speed is more effective on the front inlet side. In this study, the maximum flow rate that passes through the outlet side is around 24,200 m3/h at a rotor speed of 3000 rpm. So, to increase the flow rate at both the rear inlet and the outlet side can be done by enlarging the rear inlet rotor diameter.

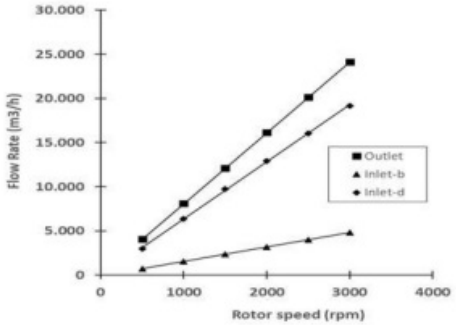

Figure 7. Effect of rotor speed on the air flow rate using the Spalart-Allmaras model

6. Conclusion

In this study, calculations have been carried out using the finite volume method to study the effect of the turbulence models and the discretization scheme on the flow that occurs in the rotor dynamometer. The results of this calculation have been compared with the measurement results. Based on the comparison of volume flow rate from the rotor, the turbulence model that gives the closest results to the measurement results is the Spalart-Allmaras turbulence model. While the best discretization scheme is PISO with second-order momentum. For further model development, research should be conducted to determine the effect of other turbulent models, Reynolds Stress Model, Large Eddy Simulation, and Direct Numerical Simulation.

Experimental and computational study on heat transfer of a 150 kW aircooled eddy current dynamometer

ORIGINALITY REPORT

16%	14%	7%	0%
SIMILARITY INDEX	INTERNET SOURCES	PUBLICATIONS	STUDENT PAPERS

PRIMARY SOURCES

1	seminarprojects.blogspot.com Internet Source	6%
2	www.scribd.com Internet Source	3%
3	file.scirp.org Internet Source	1%
4	Aljuwayhel, N.F.. "Parametric and internal study of the vortex tube using a CFD model", International Journal of Refrigeration, 200505 Publication	1%
5	tr.scribd.com Internet Source	1%
6	S. Hall, M. Cooke, A. El-Hamouz, A.J. Kowalski. "Droplet break-up by in-line Silverson rotor–stator mixer", Chemical Engineering Science, 2011 Publication	1%
7	www.cfd-online.com Internet Source	

		1%
8	www.tdx.cat Internet Source	1%
9	mafiadoc.com Internet Source	<1%
10	Hesham El-Batsh. "Numerical study of the flow field through a transonic linear turbine cascade at design and off-design conditions", Journal of Turbulence, 2006 Publication	<1%
11	eprints.undip.ac.id Internet Source	<1%
12	www.fme.vutbr.cz Internet Source	<1%
13	scholar.uwindsor.ca Internet Source	<1%
14	Aircraft Engineering and Aerospace Technology, Volume 79, Issue 3 (2007-05-20) Publication	<1%
15	etd.lib.metu.edu.tr Internet Source	<1%
16	Guo, Li, and Ronaldo G. Maghirang. "Numerical Simulation of Airflow and Particle Collection by Vegetative Barriers", Engineering Applications	<1%

of Computational Fluid Mechanics, 2012.

Publication

Exclude quotes	Off	Exclude matches	Off
Exclude bibliography	Off		

Experimental and computational study on heat transfer of a 150 kW aircooled eddy current dynamometer

GRADEMARK REPORT

FINAL GRADE

/0

GENERAL COMMENTS

Instructor

PAGE 1

PAGE 2

PAGE 3

PAGE 4

PAGE 5

PAGE 6

PAGE 7

PAGE 8

PAGE 9

PAGE 10